Intermediate valence in Yb compounds probed by 4*f* photoemission and resonant inelastic x-ray scattering

K. Kummer,[1,2] Yu. Kucherenko,[2,3] S. Danzenbächer,[2] C. Krellner,[4] C. Geibel,[4] M. G. Holder,[2] L. V. Bekenov,[3] T. Muro,[5] Y. Kato,[5] T. Kinoshita,[5] S. Huotari,[1] L. Simonelli,[1] S. L. Molodtsov,[6] C. Laubschat,[2] and D. V. Vyalikh[2]

[1]*European Synchrotron Radiation Facility, 6 Rue Jules Horowitz, B.P. 220, FR-38043 Grenoble Cedex, France*

[2]*Institut für Festkörperphysik, Technische Universität Dresden, DE-01062 Dresden, Germany*

[3]*Institute for Metal Physics, National Academy of Science of Ukraine, UA-03142 Kiev, Ukraine*

[4]*Max-Planck-Institut für Chemische Physik fester Stoffe, DE-01187 Dresden, Germany*

[5]*SPring-8, Japan Synchrotron Radiation Research Institute, Hyogo 679-5198, Japan*

[6]*European XFEL GmbH, Albert-Einstein-Ring 19, DE-22761 Hamburg, Germany*

(Received 18 July 2011; revised manuscript received 10 November 2011; published 13 December 2011)

Experimental data from 4*f* photoemission and resonant inelastic x-ray scattering experiments on the intermediate valent compound $YbRh_2Si_2$ have been compared with results of theoretical simulations. It was found that the high-energy excitations inherent to these techniques affect the spectral intensities related to different 4*f* configurations differently. Although the final states in 4*f* photoemission and x-ray absorption or resonant inelastic x-ray scattering are rather unalike, a comparable influence was found for both cases. Higher occupied 4*f* shells seem to be energetically favored in the excited states and appear overemphasized in the spectrum as compared to the ground state. For a quantitative Yb valence determination from x-ray spectroscopies, diagrams are suggested that seem to be applicable also for other intermediate valent Yb compounds.

DOI: 10.1103/PhysRevB.84.245114 PACS number(s): 71.28.+d, 71.27.+a, 71.15.Qe, 71.20.Eh

I. INTRODUCTION

Rare-earth (RE) intermetallic systems have attracted considerable interest in recent years because they exhibit many of the properties that today's solid-state research is most concerned with. Different types of magnetic ordering, superconductivity, pronounced non-Fermi-liquid behavior, quantum criticality, and heavy-fermion and Kondo behavior have been reported.[1–5] The peculiarity of RE intermetallics is the strongly localized 4*f* shell of the RE ions that lies deep inside the ionic core and maintains most of its atomic character in the solid.[5] Interaction with itinerant valence states may, however, lead to instability of the 4*f* shell and nonintegral 4*f* occupancies denoted as intermediate valent behavior.[6] This phenomenon may be described in the light of the Anderson model by means of electron hopping between itinerant valence states and localized *f* states, and leads to a mixing of different 4*f* configurations in the ground state.

The mean valence and its changes as a function of external parameters such as temperature, pressure, or chemical doping are closely related to the underlying interactions between 4*f* and valence states. Knowing the RE valence is, therefore, of crucial importance for an understanding of the underlying phenomena. 4*f* photoemission (PE) spectroscopy and resonant inelastic x-ray scattering (RIXS) or partial fluorescence x-ray absorption spectroscopy (XAS) are very sensitive to different 4*f* configurations in a RE compound that lead to characteristic signals in the spectra and form an ideal key for the experimental determination of the valence.[7–14]

On the downside, these x-ray methods involve high-energy excitations that usually end up with a strongly disturbed final state as compared to the ground state that one is interested in. Unfortunately, however, particularly in the case of heavy RE systems, respective analyses are often omitted, and the spectra are taken as a direct evidence for the valence of the ground state, leading to different results for the individual spectroscopic methods.[8]

In this paper, we discuss these effects for Yb compounds taking the heavy-fermion system $YbRh_2Si_2$ as a typical example. It is shown that for PE, XAS, and RIXS, proper application of the single-impurity Anderson model (SIAM) leads to consistent results that agree well with the low-energy properties of the system. Respective diagrams are presented that allow for a correct determination of the valence from measured intensities for all Yb systems.

II. 4*f* PHOTOEMISSION: MODEL CONSIDERATIONS

In the beginning, we analyze the 4*f* PE processes in Yb and Ce systems using simple theoretical models. As a free atom, Ce reveals a formal trivalent $[Xe]4f^1(5d6s)^3$ configuration, where trivalent refers to the number of valence electrons. In a solid, intermediate valence is obtained by admixing the neighboring $4f^0$ and $4f^1$ configurations. In the SIAM, the intermediate ground state is obtained by considering $4f^0$, $4f^1$, and $4f^2$ states at energies 0, ϵ_f, and $2\epsilon_f + U_{ff}$. Allowing for electron hopping by introducing an off-diagonal hybridization matrix element Δ and diagonalizing the model Hamiltonian yield to hybrid states of the form

$$|s\rangle = \sum_k c_{ks}|4f^{(k)}\rangle, \tag{1}$$

where the state with a minimal energy E_g is the ground state $|g\rangle$. Yb atoms, on the other hand, are characterized by a formal divalent $[Xe]4f^{14}(5d6s)^2$ configuration, and the intermediate valent ground state is generated by admixture of the trivalent $4f^{13}$ configuration. This ground state may be described in the same way as for Ce by simply considering 4*f* holes instead of 4*f* electrons. However, as it is shown in the following, Yb

and Ce systems reveal quite different behavior with respect to the assumptions and approximations made in the theoretical models, so that the model considered as acceptable for Ce systems fails to describe Yb systems, and vice versa.

A straightforward way of probing the occupancy of the RE $4f$ shell is looking at the $4f$ PE spectra. In the case of a stable $4f^n$ ground state, PE generates an electron removal state characterized by an atomiclike $4f^{n-1}$ final-state multiplet at a binding energy (BE), which corresponds to the energy necessary to increase the valence of the respective RE ion by one. PE spectra of an intermediate valent Ce or Yb ground state reveal the coexistence of two different final-state multiplets separated in energy by the on-site Coulomb repulsion energy U_{ff} between the $4f$ electrons. Since one of these final states is energetically degenerated with the ground state, its BE equals zero and the multiplet appears in the spectra at the Fermi energy E_F. This is illustrated in Fig. 1(a) for the case of $YbRh_2Si_2$ (Ref. 15) and $CeCu_2Si_2$. In the Yb compound, the coexistence of a $4f^{13}$ final-state doublet at E_F and a broad $4f^{12}$ multiplet between 6 and 12 eV BE is observed in the PE spectrum. For the Ce compound, the coexistence of $4f^0$ and $4f^1$ configurations is expected in the final state, reflected by a peak at about 2 eV BE and a $4f^1$ spin-orbit doublet at E_F, respectively.

Starting from the intermediate valent ground state, but neglecting hybridization in the final states, one expects an energy distribution function

$$I(\epsilon) \sim \sum_k k\,|c_k|^2\,\delta[\epsilon - (E_g - E_{k-1})], \tag{2}$$

where the intensities of the individual $4f^{k-1}$ final states are given by the weights $|c_k|^2$ of the $4f^k$ configurations in the ground state [ground-state picture (GSP)].

Applied to the Yb compound, one expects $4f^{13}$ and $4f^{12}$ final states with intensities $I^{(2+)}$ and $I^{(3+)}$, respectively, as it is shown in the left panel of Fig. 1(b). On this stage, the multiplet and spin-orbit splittings have been neglected for simplicity. From the measured intensities, the mean valence may be then calculated according to[8]

$$v = 3 - \frac{I^{(2+)}/14}{I^{(2+)}/14 + I^{(3+)}/13}. \tag{3}$$

Unfortunately, the GSP breaks down when Ce systems are considered, where the experimentally observed large intensity of the $4f^1$ at E_F is not in accordance with the weak contributions expected from photoionization of the $4f^2$ admixture to the ground state [see the right panel of Fig. 1(b)]. Another problem lies in the fact that the $4f^0$ admixture to the ground state has no counterpart in the final state although its contribution to the ground state is expected to be even larger than the one of the $4f^2$ configuration. Obviously, the mean valence of Ce systems can not be determined in the manner as it has been done in Eq. (3) for the Yb compound.

The mistake lies in Eq. (2) where the spectral function was assumed to consist of a simple superposition of atomiclike $4f^k$ configurations. However, if we treat the ground state as a hybrid state, the same arguments hold also for the individual final states. Particularly, the $k = 2$ component in Eq. (2) does not correspond to an atomic $4f^1$ final-state

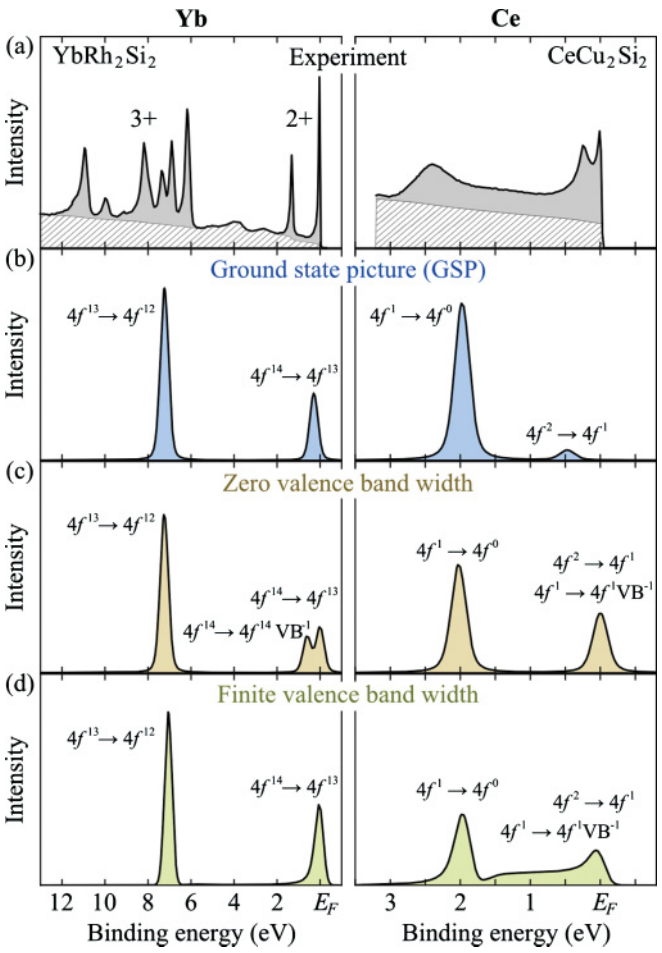

FIG. 1. (Color online) (a) Experimental $4f$ photoemission spectra from an intermediate valent Yb and an intermediate valent Ce compound (gray shaded area) compared with predictions made by (b) the ground-state picture, i.e., neglecting final-state effects [Eq. (2)], (c) taking into account final-state effects [Eq. (4)] with zero VB width, and (d) a more realistic model with a finite VB width. The used model parameters were $\epsilon_f = -0.05$ eV, $\Delta = 0.3$ eV for Yb, $\epsilon_f = -1.5$ eV, $\Delta = 1$ eV for Ce, and U_{ff} =7 eV.

configuration, but reveals the same atomic $4f^0$ and $4f^2$ admixtures like the ground state, while the $k = 1$ component reveals respective admixtures from atomic $4f^1$ and $4f^2$ configurations. Consequently, if we consider $4f$ PE from one of the $4f^k$ components in Eq. (1), the resulting $4f^{k-1}$ intensity is not determined by the $4f^k$ contribution alone, and this configuration contributes also to all other peaks observed in the PE spectrum.

Thus, the hybridization effects in initial and final states should be considered on equal footing, and then the spectral function is obtained by projecting the hole state generated by the PE process onto the individual final states:

$$I(\epsilon) \sim -\mathrm{Im} \sum_f \frac{|\langle f|\hat{T}|g\rangle|^2}{h\nu - \epsilon - (E_f - E_g) + i\Gamma}. \tag{4}$$

Here, $|g\rangle$ means the ground state and the sum should be calculated over all final states $|f\rangle$ with one electron removed. ϵ is the photoelectron kinetic energy and Γ represents the spectral broadening due to finite lifetime of the excited final

state. The dipole transition operator $\hat{T}$ in the matrix element depends in general on the photon energy $h\nu$.

The result obtained with Eq. (4) for Ce, using the simplest version of the SIAM (Ref. 16) where the valence states are assumed to form a single strongly degenerated level at E_F, is shown in the right panel of Fig. 1(c) and reveals a much larger peak at E_F in agreement with the experiment. The final-state hybridization between $4f$ and valence band (VB) states introduces a deexcitation channel for the photoexcited $4f$ shell, in addition to $4f^{(k)} \rightarrow 4f^{(k-1)}$ ionization. This channel can be described as photoemission of a $4f$ electron, but under simultaneous hopping of a valence electron into the generated $4f$ hole ($4f^{(k)} \rightarrow 4f^{(k)}\mathrm{VB}^{-1}$). Note, however, that this denotes something different than direct photoemission from a valence state, $\mathrm{VB} \rightarrow \mathrm{VB}^{-1}$, because of the participation of the $4f$ shell.

While this model, proposed by Imer and Wuilloud,[16] has been applied successfully to Ce systems, it fails to describe Yb spectra. The simulated spectrum shows the two $4f^{14} \rightarrow 4f^{13}$ and $4f^{13} \rightarrow 4f^{12}$ ionization peaks that are expected from the experiment. In addition, however, there is a third peak, the $4f^{14} \rightarrow 4f^{14}\mathrm{VB}^{-1}$ hybridization peak, that is not observed experimentally [see the left panel of Fig. 1(c)]. At first sight, the agreement with the experiment seems worse than in the GSP.

However, the sharp hybridization peak is artificial and arises due to the simplified description of the unhybridized $4f^0$ configuration in the Imer-Wuilloud model as a single VB state at E_F. In reality, the valence band is extended over a certain energy range, which makes the $4f^{(i)} \rightarrow 4f^{(i)}\mathrm{VB}^{-1}$ hybridization peak blur in the spectrum. To account for this, we have repeated the simulations within a minimal version of Gunnarsson-Schönhammer model[17] with a finite VB width. The results are shown in Fig. 1(d). The simulated spectra agree extremely well with the experimental observations, noting again that multiplet effects and spin-orbit splittings are not accounted for in these simple models. Compared to Fig. 1(c), the $4f^{(k)} \rightarrow 4f^{(k)}\mathrm{VB}^{-1}$ intensity in Yb compound got smeared out over the whole VB width.

In the next section, quantitative relations between experimentally observed spectral intensities and the Yb valence are established on the basis of simulations of spectra for $YbRh_2Si_2$.

III. YB VALENCE AND SPECTRAL INTENSITIES

A. Theoretical simulation of spectra

All PE as well as RIXS spectra presented in this paper are interpreted theoretically on the basis of the SIAM. A variational solution for the Anderson Hamiltonian may be obtained by a simple numerical procedure[17] that represents a minimal version of the Gunnarsson-Schönhammer approach.[18] Taking into account the nearly filled $4f$ shell of Yb, we used a hole representation of the code considering f^{14}, f^{13}, and f^{12} configurations as basis functions. The code was additionally generalized to take into account multiplet effects. The calculations were performed using the following parameters: the energy of a one-hole state $\epsilon_f = -0.05$ and 0.05 eV for mainly trivalent and divalent Yb atoms, respectively; the Yb $4f$ shell spin-orbit splitting 1.28 eV; the on-site Coulomb repulsion

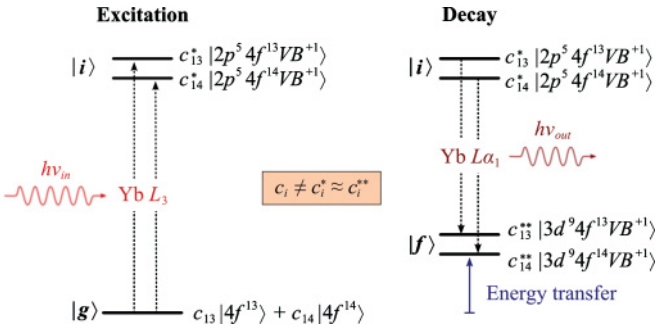

FIG. 2. (Color online) Energy scheme of the excitation and the decay processes in the RIXS experiment.

energy $U_{ff} = 6$ eV; the calculated energies and intensities of the $4f^{12}$ multiplet components were taken from Ref. 19; the valence-band density of states (DOS) for $YbRh_2Si_2$ was determined by linear muffin-tin orbital (LMTO) band-structure calculations where the Yb $4f$ were considered as core levels. For SIAM calculations, only those VB states were taken into account that are not forbidden to be hybridized with Yb $4f$ states, i.e., the local VB f components on the Yb site. Then, the hybridization parameter Δ was varied in order to change the occupancy of the Yb $4f$ shell and thus the valence of the Yb atoms.

The PE process was described by the spectral density (4), whereas RIXS spectra were calculated using the Kramers-Heisenberg relation[20]

$$I(h\nu_{\mathrm{in}}, h\nu_{\mathrm{out}}) = \sum_f \left| \sum_i \frac{\langle f|\hat{T}|i\rangle \langle i|\hat{T}|g\rangle}{E_g + h\nu_{\mathrm{in}} - E_i - i\Gamma_i} \right|^2 \times \delta(E_g + h\nu_{\mathrm{in}} - E_f - h\nu_{\mathrm{out}}), \quad (5)$$

with $\hat{T}$ the dipole transition operator, and Γ_i the spectral broadening due to the core-hole lifetime in the intermediate state. The ground, intermediate, and final states in the RIXS process for the intermediate valent Yb compound are shown in Fig. 2.

The calculations of the RIXS spectra were performed as follows: for a given set of the model parameters and fixed excitation energies $h\nu_{in}$ the intensity distributions $I(h\nu_{out})$ were calculated [constant excitation energy mode (CXE)]. The chosen values of the excitation energy cover an energy region of 40 eV around the $2p \rightarrow$ VB absorption threshold. The calculated data can be easily transformed into $I(h\nu_{\mathrm{in}})$ spectra for fixed $h\nu_{\mathrm{out}}$ values [constant emission energy mode (CEE)]. The core-hole states were accounted for in the SIAM by a parameter U_{fc} that represents the Coulomb interaction energy between a $4f$ electron and the core hole. This parameter was taken equal to 8.6 and 8.0 eV for the $2p$ and the $3d$ holes, respectively.

In our simulations, we can controllably drive the ground state from the trivalent into the intermediate valent regime by gradually increasing the hybridization strength Δ. As a result, we yield the number of $4f$ electrons in the ground state and the resulting Yb $4f$ photoemission spectrum with integral

intensities $I^{(2+)}$ and $I^{(3+)}$. In this way, both the Yb valence v and the relative intensity of the 2+ line

$$\eta = \frac{I^{(2+)}}{I^{(2+)} + I^{(3+)}} \tag{6}$$

are obtained and a quantitative relation between them can be established.

B. $v - \eta$ diagrams for PE and RIXS

In the GSP, the relative intensity η closely follows the Yb valence per definition

$$(3) = v \approx 3 - \eta. \tag{7}$$

However, beyond the GSP, when final-state effects are taken into account, the simple expression (7) is not valid.

We illustrate the results of our PE simulations for three values of Δ in Fig. 3(a), each time stating the respective Yb valence in the ground state. The full results are summarized in Fig. 3(b) where the relative intensity η of the 2+ doublet at E_F is plotted as a function of the Yb ground-state valence. The curvature reveals a significantly nonlinear dependence of the PE intensity on the ground-state valence. For comparison, the relation (3), which is assumed in the GSP, is shown as a dotted line. It runs very close to the linear dependence $\eta = 3 - v$ [cf. Eq. (7)]. Our results strongly suggest that the analysis within the GSP systematically and notably overestimates the 2+ admixture to the ground-state valence. For example, if the relative intensity of the 2+ doublet is estimated as 20% of the full $4f$ intensity, then (3) yields a valence $v \approx 2.81$, whereas our simulations suggest a value close to 2.89 [cf. arrows in Fig. 3(b)]. Note that this deviation increases if the Yb intermediate valent state is further away from the trivalent one.

Our calculations have been performed for the specific case of $YbRh_2Si_2$. Therefore, it seems interesting to ask how general our results are and if they can be transferred to other intermediate valent Yb compounds as well. To answer this, we have repeated our calculations for different, sensible sets of input parameters ϵ_f and Δ as well as for different model DOS (constant, elliptic, etc.; bandwidth $\gg\Delta$). In all cases, there have been no noteworthy deviations from the results shown in Fig. 3(b). This suggests that the found curve is applicable to Yb compounds in general and might serve as a universal gauge curve to relate experimental Yb $4f$ PE intensities to ground-state valences. It is well described by the following cubic polynomial:

$$v(\eta) = 3 - 0.55\eta - 0.01\eta^2 - 0.44\eta^3, \tag{8}$$

which we obtained from a least-squares fit of the simulated data.

In Yb $L_{2,3}$ RIXS spectra, the resonances of the divalent and trivalent Yb configuration reach their maxima at different incident photon energies $h\nu_{\text{in}}$. This difference is typically of the order of several eV. The reason is a different screening of the $2p$ core hole: $2p \rightarrow$ VB electron transition requires less energy in the divalent ($4f^{14}$) Yb ion than in the trivalent ($4f^{13}$) Yb ion (cf. Fig. 2). In contrast to that, the energy of Yb $3d \rightarrow 2p$ decay $h\nu_{\text{out}}$ does not depend on the $4f$ occupancy because both the $2p$ and the $3d$ core holes are localized within the $4f$ shell. Thus, the 2+ and 3+ peaks can be easily discriminated in RIXS because their maxima belong to the same CEE spectrum, but at different excitation energies. The absolute maximum of the spectral distribution is $I^{(3+)}$ because the considered Yb system is mainly trivalent. On the other hand, considering the RIXS spectrum in CXE mode at the excitation energy of the 2+ peak, we touch the 3+ resonance only marginally and its intensity becomes comparable to that of the 2+ line. Therefore, the CXE mode is preferable for fitting the experimental data in cases where the 2+ line is only weak, as in $YbRh_2Si_2$.

The most straightforward approach is to use again the GSP and identify the measured intensities of the 2+ and the 3+

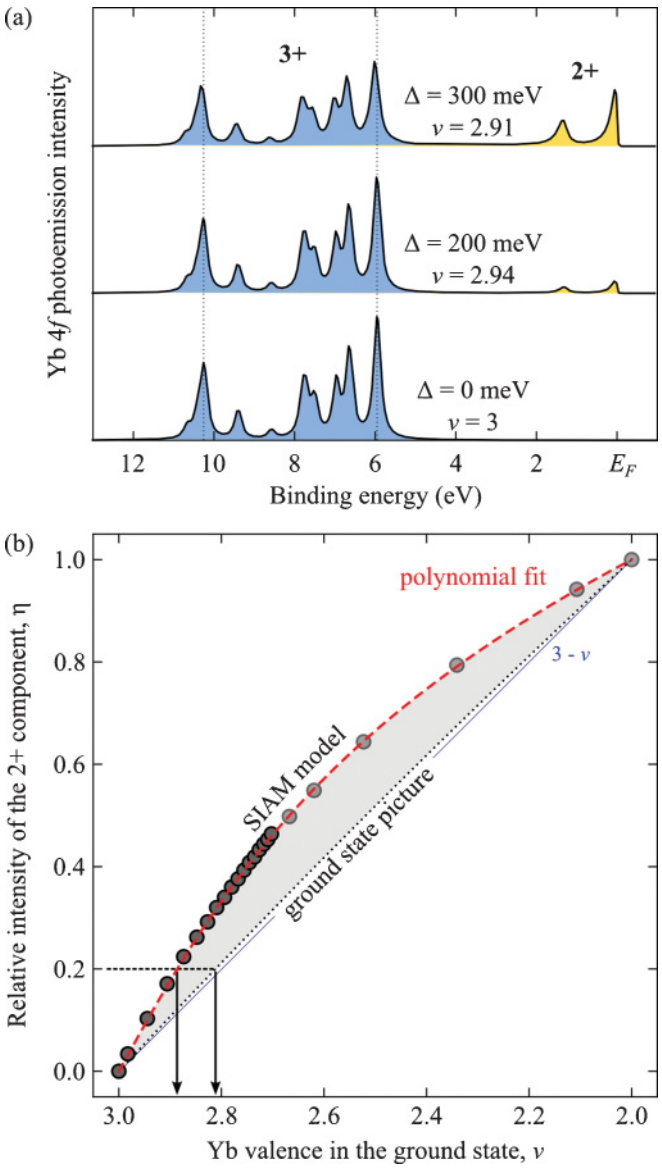

FIG. 3. (Color online) (a) $4f$ photoemission spectra simulated within the SIAM for three different hybridization strengths Δ. (b) Dependence of the relative intensity of the 2+ ($4f^{14} \rightarrow 4f^{13}$) component on the Yb valence in the ground state. The dotted line shows the prediction made by the GSP [Eq. (3)], and the filled circles show the results of our simulations. They are well described by a cubical polynomial [red dashed line, Eq. (8)].

resonances with the admixture of 2+ and 3+ Yb character. Then, the valence should immediately follow from the spectral intensities according to

$$v = 3 - \eta = 3 - \frac{I^{(2+)}}{I^{(2+)} + \zeta I^{(3+)}} \tag{9}$$

with $\zeta = 1$ for the CEE scan and $\zeta < 1$ for the CXE scan, accounting for the reduced 3+ intensity in the CXE scan through the 2+ resonance.

This could be a sensible assumption since XAS and RIXS do not directly access the $4f$ shell. Thus, the $4f$ occupancy might be stable during the entire excitation-decay process. On the other hand, the excited $2p^5 4f^{14}$ and $2p^5 4f^{13}$ intermediate states are energetically well separated, with the $4f^{14}$ configuration energetically preferred due to its better core-hole screening ability. Because of the possible $d \rightarrow f$ electron hopping, the 2+ line thus might enter overemphasized into the spectra.

We tested this assumption by means of the SIAM. The evolution of $L\alpha_1$ fluorescence spectrum with increasing Δ is shown in Fig. 4(a) for the CXE cut at the excitation energy of the 2+ peak maximum. The quantitative relation between the Yb valence and the RIXS intensities of the 2+ and 3+ resonances is plotted in Fig. 4(b) for both the CEE and the CXE scans. Comparing with the dependence (9) assumed in the GSP, one can observe clear deviations (shaded areas). Evidently, the 2+ weight in the spectrum is larger than the divalent admixture to the Yb ground state. Therefore, the GSP systematically overestimates toward the divalent Yb configuration for the above reasons. The found nonlinear dependence of $v(\eta)$ is well fitted by the quadratic polynomial (for CEE scans)

$$v(\eta) = 3 - 0.59\eta - 0.41\eta^2, \tag{10}$$

which can be useful to estimate Yb ground-state valences from spectral intensities. One can use the same polynomial for CXE scans with $\zeta = 0.13$ for the reasons discussed above [cf. Eq. (9)]. The value of ζ has been estimated from the experimental spectra as explained below.

In summary, we have quantified the final-state effects in $4f$ PE as well as L_3 edge XAS and RIXS spectra of intermediate valent Yb compounds. It was found that the typically assumed proportionality between spectral intensities and the Yb ground-state valence, i.e., (3), overestimates toward the divalent side. This has severe implications for the analysis of experimental spectra. Compared to $4f$ PE, the final-state effects in RIXS are less pronounced.

We have not extended our calculations to other RE elements yet. But, similar effects are expected for them as well. In fact, the hybridization effects might be even larger for the lighter REs since their $4f$ states are generally less strongly localized and have more overlap with the VB states.

IV. EXPERIMENTAL RESULTS AND DISCUSSION

A. Experimental details

$YbRh_2Si_2$ single crystals of about $2 \times 2 \times 1$ mm^3 size have been used as samples. The single crystals have been extensively characterized by Laue diffraction, specific heat, magnetization, and resistance measurements prior to the experiments, which evidenced excellent sample quality.[21,22] The same kinds of samples have already been subject to a number of previous angle-resolved PE spectroscopy (ARPES) studies, where they have been characterized extensively with respect to their electronic structure and demonstrated their excellent crystal quality as well.[15,23–25]

For the PE experiments, the samples were cleaved *in situ* under ultrahigh vacuum with the pressure better than 3×10^{-10} mbar. The layered structure of the samples allows us to obtain atomically clean surface after top-post cleavage. For the measurements, we tried to use areas on the sample with the silicon terminated surface in order to avoid the two additional, broad $4f$ lines in the spectrum that derive from the surface terminated with divalent Yb atoms.[26] For the RIXS measurements, the single crystals were fixed with silver paint to the sample holder and measured without any further preparation.

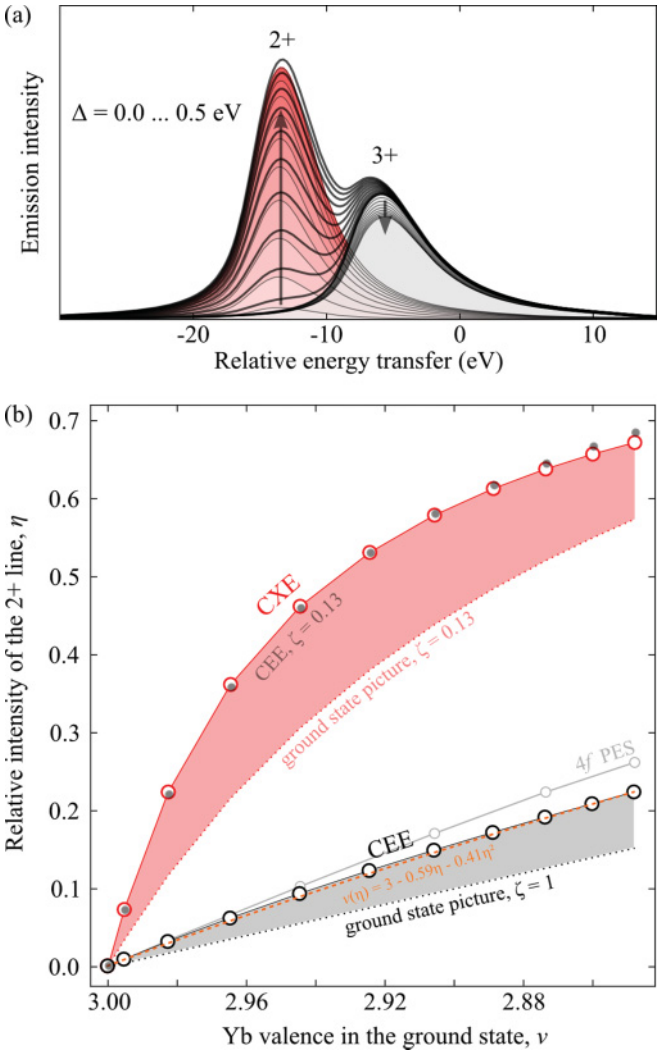

FIG. 4. (Color online) (a) Evolution of the calculated spectral intensity along the CXE cut with increasing Δ. (b) Relative intensity of the 2+ resonance line in the CEE and the CXE scans as a function of Yb valence in the ground state. The open circles show the results of our simulations, and the dotted lines the prediction made by the GSP.

Yb $4f$ PE spectra taken between 115 and 800 eV photon energy have been recorded at beamline BL25SU of the SPring-8 facility. The sample temperature was about 15 K. The total energy resolution of the spectrometer depends on the photon energy and varied between 80 and 250 meV. All spectra have been taken in angle-integrated mode. The acceptance angle of the analyzer was 12°, covering ∼15% of the Brillouin zone in the soft x-ray range. RIXS data were taken at beamline ID16 of the ESRF, using the low-resolution RIXS spectrometer. The sample temperature was set to around 10 K. The total energy resolution of the spectrometer was about 1.5 eV.

B. $4f$ photoemission spectroscopy

Aside from the nonlinear relation between the admixture of the different $4f$ configurations to the ground state and the intensities of the respective $4f$ PE lines, there is still the problem of accurate experimental estimation of the $4f$ PE intensities of the 2+ and 3+ peaks. Here, the main issues that must be dealt with are a proper consideration of the non-$4f$ background and the surface sensitivity of the PE process.

Background subtraction. In a $4f$ PE experiment, the $4f$-derived signals are superimposed by VB emissions and a background of inelastically scattered electrons that have to be considered in order to analyze the $4f$-derived spectral function. Usually, the VB contributions are simply subtracted, whereby their actual shape is derived from the comparison of PE spectra taken at different photon energies, exploiting the different dependence of the $4f$ and VB photoionization cross sections on the excitation energy. Unfortunately, the cross sections of the VB states vary as a function of their angular momentum character, and upon subtraction of the VB contributions, there arises the problem of normalization. Particularly for Ce compounds, this is a severe problem since there are strong $4f$-derived contributions in the region of the VB emission [cf. the right panel of Fig. 1(d)], which reveal a similar shape as the latter but must not be removed accidentally by the subtraction procedure. For Yb compounds, the situation is much simpler: the narrow features of the $4f^{13}$ doublet may easily be identified, while in the BE region of the broad $4f^{12}$ multiplet there are usually no overlapping VB contributions. Between them, respective $4f$ contributions are practically lacking [cf. the left panel of Fig. 1(d)] due to small ϵ_f and Δ values as compared to the width of the VB, while in Ce systems, both are of the same order of magnitude. Moreover, since the spectral intensity of $4f$ emissions is proportional to the $4f$ occupation, it is large in the case of Yb systems. In order to consider the contribution of inelastically scattered electrons, an integral background has been subtracted from the spectra adjusted in a way that the high-BE tails of the $4f^{12}$ multiplet are fully suppressed. We are aware of the fact that, due to this background subtraction, also the inherent symmetry of the PE lines is affected. However, the latter is small for most Yb systems and its effect on the relative PE intensity is weak, if all PE lines are treated in the same way.

Surface sensitivity. The short mean-free path of electrons in a solid restricts PE to the first few atomic layers. In the recent past, advances started to increase the probing depth of photoemission by going to higher photon energies, i.e., the soft and hard x-ray ranges.

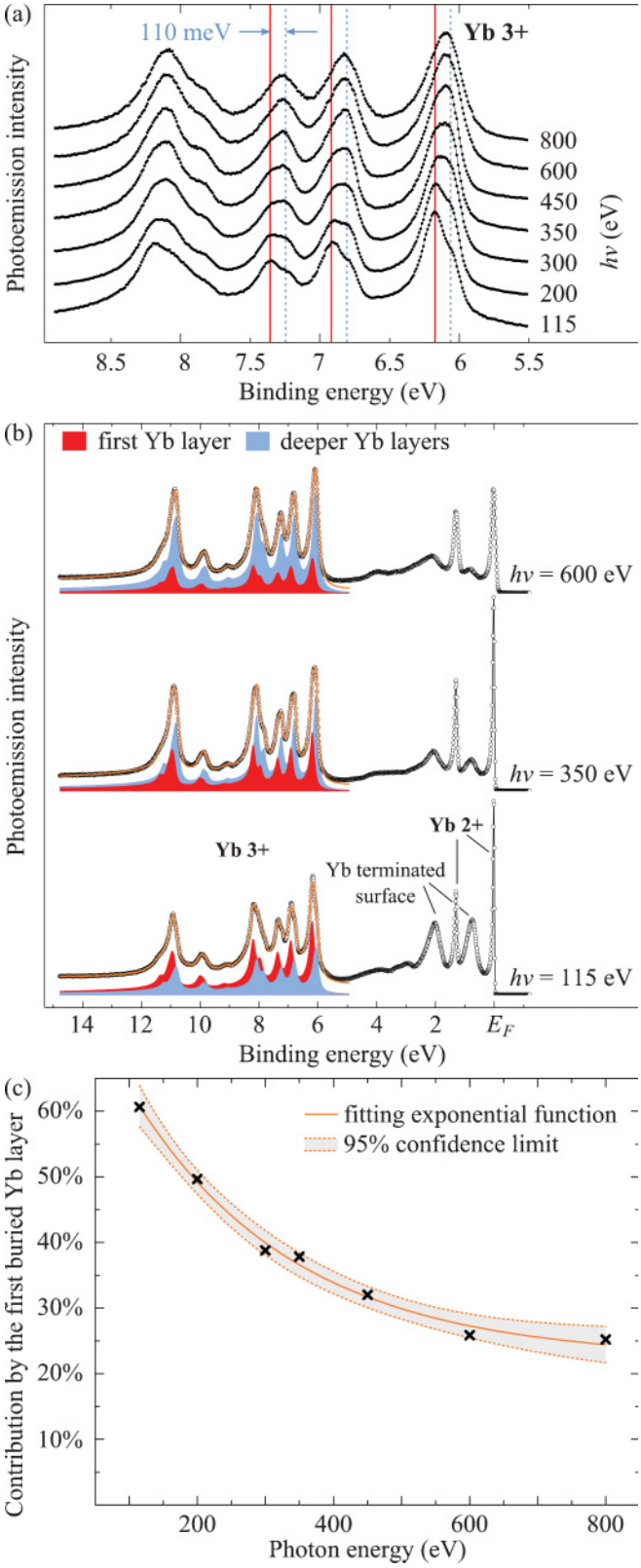

FIG. 5. (Color online) (a) Zoom-in into a part of the 3+ multiplet for a series of spectra, taken with increasing photon energy, revealing considerable lineshape variations. (b) Intensity changes with photon energy of the 3+ multiplets assigned to subsurface and deeper (bulk) Yb layers. (c) Relative contribution of the subsurface Yb layer to the overall $4f$ photoemission with increasing photon energy.

Figure 5(a) shows a series of PE spectra taken from $YbRh_2Si_2$ with gradually increasing photon energy. The displayed BE range between 5.5 and 8.5 eV covers the low-BE part of the $4f^{13} \rightarrow 4f^{12}$ (3+) multiplet, and the multiplet components show up as well-separated peaks and shoulders. Counting the individual components yields twice the number that is expected from atomic considerations.[19] In fact, having a close look at the 115-eV spectrum, the multiplet components appear to come in pairs of a more intense peak preceded by a less intense peak at ∼110 meV lower BE. At higher photon energies, the lower BE peaks grow in intensity, and in the 800-eV spectrum, they are already more intense than their partners at ∼110 meV higher BE. Note that a splitting of the 3+ component has been observed for other Yb compounds, too.[27,28]

A straightforward explanation for this could be given when different energy positions of the $4f^{13} \rightarrow 4f^{12}$ multiplet are assumed for the first buried (subsurface) and deeper-lying Yb layers.[29] The photoelectron escape depth depends on the excitation energy used, so that the relative contributions from the subsurface and from deeper Yb layers are substantially different in the 115- and the 800-eV spectra.

To test this hypothesis, we performed a least-squares-fit analysis of the $4f^{13} \rightarrow 4f^{12}$ part of all spectra in the series, always using a pair of two identical multiplet spectral functions, with the energy offset between them fixed at 110 meV. The only free parameters were the total intensities of the two multiplets and their Gaussian broadening to account for different energy resolutions at different photon energies. The results are shown in Fig. 5(b) for three selected photon energies. Obviously, there is a systematic evolution in the intensity of the two multiplets when going from the surface-sensitive regime at 115 eV to higher probing depths at 350 and 600 eV. The red colored (dark) multiplet at higher BE can be ascribed to the subsurface Yb layer and the blue colored (light) one to deeper-lying Yb layers. Following the ratio of their intensities as a function of photon energy, one can get a good estimation of surface versus bulk sensitivity of PE spectra for $YbRh_2Si_2$ and other comparable materials.

Figure 5(c) shows the relative contribution of the subsurface Yb layer to the spectrum as a function of photon energy. The data are well described by a simple exponential function, corresponding to an exponential increase of the effective attenuation length with kinetic energy.[30] Looking at the curve, the PE signal evidently becomes more sensitive to deeper-lying atomic layers for higher photon energies. At the same time, our data also suggest that, for the here studied layered type of 4f systems, surface and subsurface may still notably contribute to the spectrum, even for photon energies above 1 keV.

Discrimination of surface and bulk contributions. The contribution of both the subsurface and deeper-lying layers makes it difficult to give a good estimate of the Yb valence in either of them from a single $4f$ photoemission spectrum. While their $4f^{13} \rightarrow 4f^{12}$ (3+) contributions may be separated by means of a fit analysis, as in Fig. 5(b), the $4f^{14} \rightarrow 4f^{13}$ (2+) doublet does not exhibit any substructure. It is, therefore, impossible to distinguish between the 2+ intensity derived from the subsurface or deeper-lying layers.

Distinction may, however, become possible when the difference of two spectra, taken at rather different photon energies and suitably normalized, is considered instead. We would like to illustrate that using the 350- and 600-eV spectrum of Fig. 5(b). These two are selected only because the spectrometer resolution is rather similar, which facilitates their comparison. In order to remove all contributions of deeper-lying layers from the more surface-sensitive 350-eV spectrum, we renormalize the 600-eV spectrum so that the intensity of the blue 3+ multiplet function is equal to the intensity of the blue 3+ multiplet function of the 350-eV spectrum. If we now subtract the renormalized 600-eV spectrum from the 350-eV spectrum, the difference spectrum will contain only $4f$ contributions from the subsurface Yb layer. Similarly, we can remove the subsurface contributions from the 600-eV spectrum by renormalizing the 350-eV spectrum such that for both spectra, the intensity of the red multiplet is the same and subsequently taking the difference.

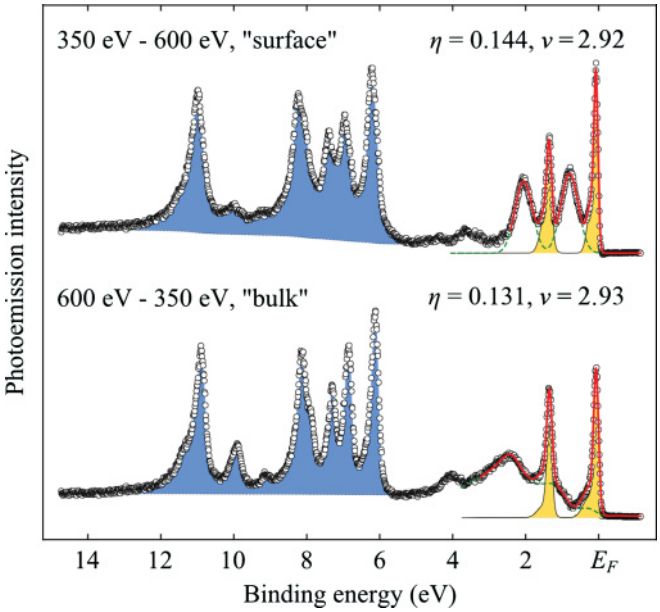

FIG. 6. (Color online) Subsurface and bulk parts of the $4f$ plus VB photoemission from $YbRh_2Si_2$ as obtained by comparison between low- and high-photon-energy data.

The resulting spectra are both shown in Fig. 6. They should correspond to the $4f$ PE from either surface and subsurface Yb or deeper-lying Yb layers. Note that the VB contributions to the difference spectra are rather different. This is an artifact of the subtraction procedure, where normalization was done with respect to the $4f$ emissions while VB contributions are not comparable to each other due to different photoionization cross sections. As a further detail, the upper difference spectrum reveals an additional $4f^{13}$ spin-orbit doublet at about 0.9 eV BE (dashed line), which is derived from divalent Yb atoms at the outermost atomic surface layer. The fact that this feature is absent in the lower difference spectrum shows that the discrimination of surface- and bulk-related features was rather successful.

Valence estimation. One can now determine the relative intensities of the 2+ line η and apply (8) to obtain the Yb valence for either case. Doing so, we yield $v = 2.92$ for the subsurface Yb layer and $v = 2.93$ for deeper-lying Yb layers.

Note that Yb atoms in the subsurface layer change their valence only slightly in comparison to the bulk Yb atoms, in spite of existing surface effects (the energy shift of the $4f^{12}$ multiplet).

In the simulated $4f$ PE spectra in Fig. 3(a), the 3+ multiplet shifts toward higher BE as Δ, and therewith the 2+ admixture, is increased. However, this effect is considerably smaller than the experimentally observed one. It may be supposed that this energy shift is caused mainly due to the changes in the VB charge distribution close to the surface and, consequently, its screening properties. Similar shifts of the 3+ component have been also observed in PE spectra where the intermediate valence in $YbRh_2Si_2$ has been varied by gradual substitution of Rh ions by Co ions.[22]

The best fit of the bulk PE spectrum shown in Fig. 6 by means of the SIAM was achieved for $\Delta = 260$ meV. From that, it is possible to estimate the Kondo temperature T_K for $YbRh_2Si_2$ within the Gunnarsson-Schönhammer scheme.[18] For $\epsilon_f = -50$ meV and the calculated width $W = 10$ eV of the occupied part of the DOS $n(E_F) = 0.0895$ eV^{-1}, we obtain a value $T_K \approx 30$ K, in fair agreement with experimental estimations $T_K \approx 24$ K.[31] Taking into account an error of about ± 10 meV for the value of Δ, the interval for the estimated T_K is between 15 and 55 K, which could still be considered a nice result. However, the critical point is the small value of ϵ_f, which is comparable to the crystal-field splitting of the Yb level in $YbRh_2Si_2$,[32] and makes its accurate estimation from the experimental data impossible. We have repeated our simulations of PE spectra using $\epsilon_f = -10$ meV yielding $\Delta = 120$ meV for the best fit with no significant effect on the results for Yb valence, as presented above. But, the accuracy interval for T_K (using the same error of ± 10 meV for Δ) is now between 10 and 160 K. Thus, the small values of ϵ_f and Δ for Yb make it extremely difficult to relate the high-energy scales and the low-energy (Kondo) scale to each other.

In summary, it became evident that Yb $4f$ PE spectroscopy is usually restricted to the first few atomic layers but, up to some extent, the probing depth can be enhanced by going to higher photon energies. In certain cases, it is even possible to indirectly distinguish between the subsurface and deeper-lying Yb layers by analyzing the small changes in the $4f$ PE signal as photon energy is varied. However, bulk information can only be obtained indirectly and thus may only reach a certain level of accuracy. For the above reasons, PE may sometimes have trouble to complement or repeat results that were obtained with low-energy techniques in the bulk of the material (specific heat, etc.).

C. X-ray absorption and resonant inelastic x-ray scattering

In contrast to photoemission, x-ray absorption in fluorescence yield mode and the related resonant inelastic x-ray scattering can be used as truly bulk sensitive, spectroscopic methods to measure intermediate valence in RE intermetallics. A second advantage of measuring emitted photons instead of electrons is the possibility to work under extreme conditions such as applied magnetic fields or external pressure. This allows us to study the intermediate valence in RE compounds in different regions in the phase diagram. For RE compounds, the $L_{2,3}$ absorption edges in the hard x-ray range have been found to be particularly suitable for measuring valences.[7,9,14,33–35]

Both the XAS and the RIXS approaches are very similar for the here considered type of experiment. The generic difference between $L_{2,3}$ x-ray absorption and RIXS is that for the former, the excitation ($2p \rightarrow 5d^*$) is well defined by the incident photon energy, but then all fluorescent decay channels are measured [total fluorescence yield (TFY)]. In RIXS, on the other hand, one further restricts oneself to a small energy interval in one particular decay channel, for example, the $L\alpha_1$ decay of the $2p$ core hole n the present case (see Fig. 2). This requires decent energy resolution in both the incident and the scattered beams as well as an order(s) of magnitude higher intensity for the incident beam to have a comparable photon yield. The RIXS experiment is, therefore, much more demanding. However, the natural spectral broadening is no longer defined by the lifetime of the deep $2p$ core hole[36,37] but by the much shallower $3d$ core hole.[38] This can be a decisive factor. Often, spectral components, which are already indistinguishable in TFY-XAS, can still be resolved in the RIXS spectrum.[35]

A good example is given by the two spectra in Fig. 7(a). Both were taken from the intermediate valent Yb intermetallic $YbRh_2Si_2$ at $T = 10$ K during the same scan. The gray shaded area is the TFY-XAS signal as a function of excitation energy. The white circles show the photon yield measured at 7.4125-keV emission energy in the maximum of the $L\alpha_1$ fluorescence. In the TFY spectrum, the near-edge structure appears to consist of one broad resonance at ~8.947 eV. On the contrary, the spectrum measured in the maximum of $L\alpha_1$ fluorescence reveals two well-separated resonances, and even a third resonance at lower excitation energy becomes distinguishable. These three resonances are assigned to $2p \rightarrow 5d^*$ dipole transitions in divalent (2+) and trivalent (3+) Yb ions, respectively, and the $2p \rightarrow 4f$ quadrupole transition ($E2$) in the trivalent Yb ion.

Figure 7(b) probably gives a good visual idea of why the RIXS and the XAS spectra are so different in terms of natural linewidths. It shows the photon yield from the $YbRh_2Si_2$ sample mapped as a function of excitation energy $h\nu_{in}$ and emitted energy $h\nu_{out}$ at the $L_3 - L\alpha_1$ edge. For convenience the vertical axis shows the energy transfer into the sample, $E_t = h\nu_{in} - h\nu_{out}$, instead of the energy of the scattered photons. In this representation, CEE cuts are along diagonal lines from the lower left to the upper right, whereas CXE cuts are along vertical lines. In the structure around the onset of Yb $L\alpha_1$ emission, one can find the three resonances in the CEE scan of Fig. 7(a) again: The intense 3+ peak at $h\nu_{in} = 8.947$ keV and the less intense 2+ peak at $h\nu_{in} = 8.9405$ keV, where the shown CEE and CXE lines cross. The structureless line that leaves the map to the upper right at CEE is the nonresonant fluorescence, corresponding to continuum transitions that set in at the edge jump.

Looking at the individual resonances, they are broadened significantly different along the x and the y axes, which we tried to indicate only for the 3+ resonance peak. Along the x axis, the linewidths Γ are defined by the $2p$ core-hole lifetime and along the y axis by the lifetime of the shallower $3d$ core hole. The RIXS spectrum in Fig. 7(a) corresponds to the CEE scan indicated with the line of white circles. Obviously, its

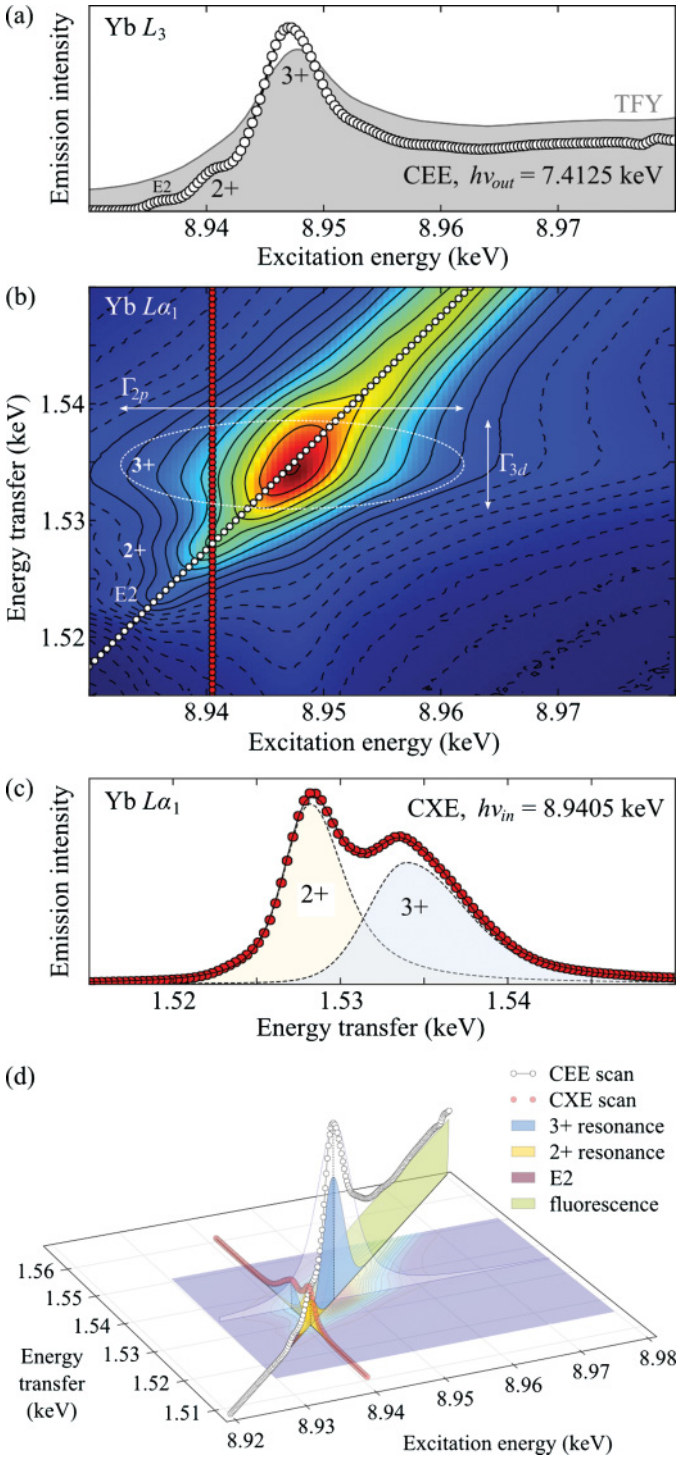

FIG. 7. (Color online) (a) TFY-XAS and RIXS spectra in CEE mode of $YbRh_2Si_2$ at $T = 10$ K. (b) Intensity map of the Yb $L\alpha_1$ fluorescence yield as a function of excitation and transferred energy. Broadening of the resonances in x and y is given by the lifetimes of the $2p$ and $3d$ core holes, respectively. The CEE and CXE cuts through the maximum of the 2+ resonance are indicated by the lines of white and red (gray) circles, respectively. (c) Emission intensity along the CXE cut indicated in (b). (d) Given by the $2p$ lifetime broadening and the excitation energy separation of the 2+ and 3+ resonances, the latter is reduced to 13% intensity in the CXE scan as compared to its intensity in the 3+ maximum.

spectral broadening is given by Γ_{3d} as long as the energy resolution in the scattered beam is higher than that. TFY-XAS does not discriminate between different emission energies, and for each excitation energy integrates intensities over the whole y axis. It therefore sees the full width Γ_{2p}.

Having energy resolution in the scattered beam can also be useful to selectively enhance the contribution of a weak resonance over a strong one.[7,8,35] Let us consider, for instance, Kondo compounds such as the here discussed $YbRh_2Si_2$, where the intermediate valence is close to 3+ but known to depend on temperature. Changing the temperature will thus affect the intensity of the 2+ resonance. However, relative to the intense 3+ resonance, the effect will be very small and hard to quantify from the spectrum shown in Fig. 7(a).

Therefore, it can be advisable to use CXE cut (red circles) in the intensity map in Fig. 7(b).[8] The resulting spectrum is shown in Fig. 7(c). The originally small 2+ resonance intensity is now comparable to that of the 3+ resonance, despite the only small divalent admixture in the ground state. This CXE spectral shape is much simpler to analyze because only the 2+ and the 3+ resonances notably contribute. This makes it easy to accurately follow small relative changes of the 2+ intensity as a function of, for instance, magnetic field, temperature, or applied pressure.[7,9,35] Unfortunately, the CXE scan gives no direct information on the intensity ratio between the 2+ and 3+ peaks in their respective resonance maxima. For this information, one has to compare with another cut that crosses the 3+ resonance in its maximum and normalize the 2+ and 3+ intensity accordingly [Fig. 7(d)]. This can be, for example, the CEE scan shown in white circles.[7] From this procedure, the value $\zeta = 0.13$ for Eq. (9) has been found.

In summary, RIXS is a very versatile method that is sensible to the different $4f$ configurations in RE intermetallic compounds. The results of our SIAM simulations can be used to translate the spectra into realistic estimates of the ground-state valence [Eq. (10)]. Figure 8 shows the simulated spectra together with the experimental $YbRh_2Si_2$ data of Fig. 7(b). Both agree well, noting that the low-excitation energy feature due to quadrupole excitations can not be reproduced with dipole transition operator $\hat{T}$.

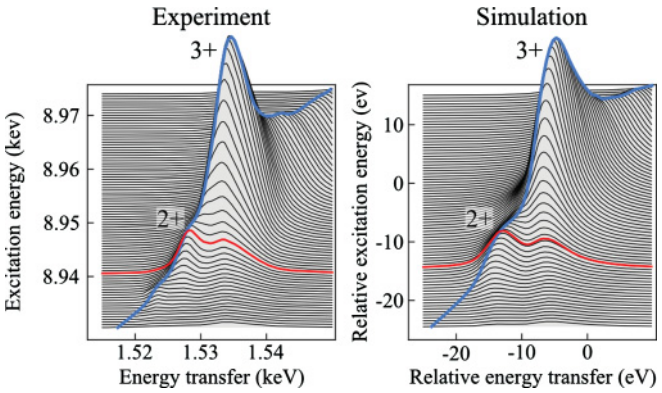

FIG. 8. (Color online) Experimental RIXS data for $YbRh_2Si_2$ at $T = 10$ K and results of SIAM simulations for hybridization strength $\Delta = 0.26$ eV. The CEE and CXE cuts are shown as blue and red lines running across and horizontal, respectively.

TABLE I. Comparison of the values for the low-temperature valence in $YbRh_2Si_2$, estimated from $4f$ PE and RIXS measurements in the GSP and after including final-state effects.

	v (GSP)	v
$4f$ photoemission	2.88	2.93
RIXS, CEE scan	2.89	2.93
RIXS, CXE scan	2.88	2.92

V. CONCLUSIONS

One of the motivations of this work was to understand why the valence estimations from different spectroscopic techniques often do not agree well with each other, or with results from low-energy excitation techniques. The main reason was anticipated in final-state effects that may be very pronounced in the considered spectroscopies. We tried to get hold of their size by performing extensive simulations in comparison with experimental data, at the specific example of the intermediate valent compound $YbRh_2Si_2$. The simulations revealed considerable final-state effects, which particularly favor the spectral features related to the $4f^{14}$ ground-state configuration. If those effects were not accounted for, the divalent admixture in the ground state would be determined as too high.

It is, of course, interesting to compare the results from x-ray spectroscopies and low-energy excitations again, now that we have tried to quantify the occurring final-state effects. We have shown and discussed low-temperature spectroscopic results for $YbRh_2Si_2$ throughout this paper and our results obtained from $4f$ PE and L_3 edge RIXS are summarized in Table I.

From thermodynamic, magnetic, and transport measurements it can only be established that v is slightly below, but close to, 3+. However, they give a quite precise measure for the Kondo scale $T_K = 20$ K, which should correspond to a valence of $v \approx 2.95$ below T_K. Thus, there is a large deviation between this estimation and the spectroscopic results obtained within the GSP (left column of Table I). However, after accounting for final-state effects, a consistent picture arises from the different techniques. This well demonstrates the impact of final-state effects on x-ray spectroscopy results. Only after their quantitative characterization may meaningful comparison or complementation of data from various techniques become possible.

Another aspect that can complicate comparison of results obtained with different techniques is the surface versus bulk sensitivity inherent to the techniques. In particular, $4f$ PE was found to preserve much of its surface sensitivity even when going to the hard x rays. However, a separation of surface and bulk signal could be tried by comparing the spectra obtained at different photon energies. In this way, we deduced a pure bulk photoemission spectrum from our experimental data, and its analysis yielded a $4f$ occupancy that agrees very well with the values that were obtained with bulk sensitive techniques.

ACKNOWLEDGMENTS

This work was supported by the DFG (Grants No. VY64/1-1 and No. GE602/2-1) and the SPring-8 facility under Proposal No. 2009A1029.

[1] Q. M. Si and F. Steglich, Science **329**, 1161 (2010).
[2] P. Gegenwart, T. Westerkamp, C. Krellner, Y. Tokiwa, S. Paschen, C. Geibel, F. Steglich, E. Abrahams, and Q. Si, Science **315**, 969 (2007).
[3] J. Custers, P. Gegenwart, H. Wilhelm, K. Neumaier, Y. Tokiwa, O. Trovarelli, C. Geibel, F. Steglich, C. Pepin, and P. Coleman, Nature (London) **424**, 524 (2003).
[4] G. R. Stewart, Rev. Mod. Phys. **73**, 797 (2001); **78**, 743 (2006).
[5] G. R. Stewart, Rev. Mod. Phys. **56**, 755 (1984).
[6] C. M. Varma, Rev. Mod. Phys. **48**, 219 (1976).
[7] C. Dallera, M. Grioni, A. Shukla, G. Vankó, J. L. Sarrao, J. P. Rueff, and D. L. Cox, Phys. Rev. Lett. **88**, 196403 (2002).
[8] L. Moreschini, C. Dallera, J. J. Joyce, J. L. Sarrao, E. D. Bauer, V. Fritsch, S. Bobev, E. Carpene, S. Huotari, G. Vanko, G. Monaco, P. Lacovig, G. Panaccione, A. Fondacaro, G. Paolicelli, P. Torelli, and M. Grioni, Phys. Rev. B **75**, 035113 (2007).
[9] J.-P. Rueff, J.-P. Itie, M. Taguchi, C. F. Hague, J.-M. Mariot, R. Delaunay, J.-P. Kappler, and N. Jaouen, Phys. Rev. Lett. **96**, 237403 (2006).
[10] J. M. Lawrence, G. H. Kwei, P. C. Canfield, J. G. DeWitt, and A. C. Lawson, Phys. Rev. B **49**, 1627 (1994).
[11] J. M. Lawrence, A. J. Arko, J. J. Joyce, R. I. R. Blyth, R. J. Bartlett, P. C. Canfield, Z. Fisk, and P. S. Riseborough, Phys. Rev. B **47**, 15460 (1993).
[12] J. M. Lawrence, M. L. den Boer, R. D. Parks, and J. L. Smith, Phys. Rev. B **29**, 568 (1984).
[13] T. K. Sham, R. A. Gordon, and S. M. Heald, Phys. Rev. B **72**, 035113 (2005).
[14] H. Yamaoka, M. Taguchi, A. M. Vlaicu, H. Oohashi, K. Yokoi, D. Horiguchi, T. Tochio, Y. Ito, K. Kawatsura, K. Yamamoto, A. Chainani, S. Shin, M. Shiga, and H. Wada, J. Phys. Soc. Jpn. **75**, 034702 (2006).
[15] S. Danzenbächer, Yu. Kucherenko, D. V. Vyalikh, M. Holder, C. Laubschat, A. N. Yaresko, C. Krellner, Z. Hossain, C. Geibel, X. J. Zhou, W. L. Yang, N. Mannella, Z. Hussain, Z.-X. Shen, M. Shi, L. Patthey, and S. L. Molodtsov, Phys. Rev. B **75**, 045109 (2007).
[16] J.-M. Imer and E. Wuilloud, Z. Phys. B: Condens. Matter **66**, 153 (1987).
[17] R. Hayn, Yu. Kucherenko, J. J. Hinarejos, S. L. Molodtsov, and C. Laubschat, Phys. Rev. B **64**, 115106 (2001).
[18] O. Gunnarsson and K. Schönhammer, Phys. Rev. B **31**, 4815 (1985).
[19] F. Gerken, J. Phys. F: Met. Phys. **13**, 703 (1983).
[20] A. Kotani and S. Shin, Rev. Mod. Phys. **73**, 203 (2001).
[21] C. Krellner, S. Hartmann, A. Pikul, N. Oeschler, J. G. Donath, C. Geibel, F. Steglich, and J. Wosnitza, Phys. Rev. Lett. **102**, 196402 (2009).

[22]C. Klingner, C. Krellner, M. Brando, C. Geibel, F. Steglich, D. V. Vyalikh, K. Kummer, S. Danzenbächer, S. L. Molodtsov, C. Laubschat, T. Kinoshita, Y. Kato, and T. Muro, Phys. Rev. B **83**, 144405 (2011).

[23]D. V. Vyalikh, S. Danzenbächer, A. N. Yaresko, M. Holder, Yu. Kucherenko, C. Laubschat, C. Krellner, Z. Hossain, C. Geibel, M. Shi, L. Patthey, and S. L. Molodtsov, Phys. Rev. Lett. **100**, 056402 (2008).

[24]D. V. Vyalikh, S. Danzenbächer, Yu. Kucherenko, C. Krellner, C. Geibel, C. Laubschat, M. Shi, L. Patthey, R. Follath, and S. L. Molodtsov, Phys. Rev. Lett. **103**, 137601 (2009).

[25]D. V. Vyalikh, S. Danzenbächer, Yu. Kucherenko, K. Kummer, C. Krellner, C. Geibel, M. G. Holder, T. K. Kim, C. Laubschat, M. Shi, L. Patthey, R. Follath, and S. L. Molodtsov, Phys. Rev. Lett. **105**, 237601 (2010).

[26]D. V. Vyalikh, S. Danzenbächer, C. Krellner, K. Kummer, C. Geibel, Yu. Kucherenko, C. Laubschat, M. Shi, L. Patthey, R. Follath, and S. L. Molodtsov, J. Electron Spectrosc. Relat. Phenom. **181**, 70 (2010).

[27]T. Okane, S.-I. Fujimori, A. Ino, A. Fujimori, S. K. Dhar, C. Mitra, P. Manfrinetti, A. Palenzona, and O. Sakai, Phys. Rev. B **65**, 125102 (2002).

[28]H. Sato, K. Yoshikawa, K. Hiraoka, M. Arita, K. Fujimoto, K. Kojima, T. Muro, Y. Saitoh, A. Sekiyama, S. Suga, and M. Taniguchi, Phys. Rev. B **69**, 165101 (2004).

[29]Note that Yb atoms in the outermost surface layer (for Yb terminated surfaces) are purely divalent and do not contribute to the $4f^{12}$ multiplet intensity. The subsurface Yb layer is defined as the first buried Yb layer, and for Si terminated surfaces it is the fourth atomic layer from the surface.

[30]C. J. Powell and A. Jablonski, J. Phys. Chem. Ref. Data **28**, 19 (1999).

[31]O. Trovarelli, C. Geibel, S. Mederle, C. Langhammer, F. M. Grosche, P. Gegenwart, M. Lang, G. Sparn, and F. Steglich, Phys. Rev. Lett. **85**, 626 (2000).

[32]O. Stockert, M. M. Koza, J. Ferstl, A. P. Murani, C. Geibel, and F. Steglich, Phys. B (Amsterdam) **378–380**, 157 (2006).

[33]L. Journel, J. M. Mariot, J. P. Rueff, C. F. Hague, G. Krill, M. Nakazawa, A. Kotani, A. Rogalev, F. Wilhelm, J. P. Kappler, and G. Schmerber, Phys. Rev. B **66**, 045106 (2002).

[34]I. Jarrige, H. Ishii, Y. Q. Cai, J.-P. Rueff, C. Bonnelle, T. Matsumura, and S. R. Shieh, Phys. Rev. B **72**, 075122 (2005).

[35]C. Dallera, E. Annese, J.-P. Rueff, A. Palenzona, G. Vanko, L. Braicovich, A. Shukla, and M. Grioni, Phys. Rev. B **68**, 245114 (2003).

[36]U. Arpt, G. Materlik, M. Richter, and B. Sonntag, J. Phys. B: At., Mol. Opt. Phys. **23**, L811 (1990).

[37]K. Hämäläinen, S. Manninen, S. P. Collins, and M. J. Cooper, J. Phys.: Condens. Matter **2**, 5619 (1990).

[38]K. Hämäläinen, D. P. Siddons, J. B. Hastings, and L. E. Berman, Phys. Rev. Lett. **67**, 2850 (1991).